Mathematical Analysis on the Uniqueness of Reverse Algorithm for Measuring Elastic-Plastic Properties by Sharp Indentation

Yongli Huang[1)], *Xiaofang Liu*[1)], *Yichun Zhou*[1)†], *Zengsheng Ma*[1)] *and Chunsheng Lu*[2)]

1) Key Laboratory of Low Dimensional Materials and Application Technology of Ministry of Education, and Faculty of Materials, Optoelectronics and Physics, Xiangtan University, Hunan 411105, China

2) Department of Mechanical Engineering, Curtin University, Perth, WA 6845, Australia

The reverse analysis provides a convenient method to determine four elastic-plastic parameters through an indentation curve such as Young's modulus E, hardness H, yield strength σ_y and strain hardening exponent n. In this paper, mathematical analysis on a reverse algorithm from Dao model (Dao *et al.*, *Acta Mater.*, 2001, **49**: 3899) was carried out, which thought that only when $20 \le E^*/\sigma_{0.033} \le 26$ and $0.3 < n \le 0.5$, the reverse algorithm would yield two solutions of n by dimensionless function Π_2. It is shown that, however, there are also two solutions of n when $20 \le E^*/\sigma_{0.033} \le 26$ and $0 \le n < 0.1$. A unique n can be obtained by dimensionless function Π_3 instead of Π_2 in these two ranges. E and H can be uniquely determined by a full indentation curve, and σ_y can be determined if n is unique. Furthermore, sensitivity analysis on obtaining n from dimensionless function Π_3 or Π_2 has been made.

KEY WORDS: Elastic-plastic properties; Sharp indentation; Reverse algorithm; Uniqueness; Sensitivity

† Corresponding author. Tel.: +86 731 58293577;
E-mail address: zhouyc@xtu.edu.cn (Y.C. Zhou).

1. Introduction

With the rapid development of modern microelectronics and high integration of devices, mechanical properties of small-scale materials have attracted increasing attention. A good understanding on their mechanical behaviors becomes particularly indispensable in applications[1, 2]. The traditional mechanical testing can not be applicable due to small dimensions of materials. A lot of new methods, such as micro-tensile, micro-bending, micro-cantilever and instrumented indentation tests, have been developed[3−10]. Among these methods, instrumented indentation has attained an ever-increasing application due to its high resolution of displacement, real-time monitoring, and high data acquisition rate[6−10].

Figure 1 shows a typical indentation response by a sharp indenter on a metal. The loading curve can be described by the equation, $P = Ch^2$, where C is the loading curvature. The initial unloading slope $\left(\mathrm{d}P_\mathrm{u}/\mathrm{d}h\right)\big|_{h_\mathrm{m}}$ is the contact stiffness S, with P_u the unloading force and h_m the maximum displacement at the maximum load P_m. The term h_r represents the residual displacement after complete unloading. The total work is described as $W_\mathrm{t} = W_\mathrm{e} + W_\mathrm{p}$ with W_e the elastic work and W_p the plastic work. Young's modulus E and hardness H can be directly obtained from the indentation curve (see Fig. 1) by the Oliver-Pharr (O-P) method[7]. However, the O-P method can only deal with the sink-in phenomena, and if pile-up occurs, it may overestimate E and H[11, 12]. Furthermore, elastic-plastic properties of a material cannot completely be characterized by Young's modulus and hardness. The plastic behavior of a homogeneous and isotropic metal is usually described by a power-law stress-strain (σ-ε) relationship, which can be expressed as[13]:

$$\sigma = E\varepsilon \quad \text{for} \quad \sigma \le \sigma_\mathrm{y} \quad \text{and} \quad \sigma = R\varepsilon^n \quad \text{for} \quad \sigma \ge \sigma_\mathrm{y} \tag{1}$$

where σ_y is the yield stress, $R = \sigma_\mathrm{y}(E/\sigma_\mathrm{y})^n$ is a strength coefficient, and n is the strain hardening exponent. When plastic deformation occurs, the total strain ε can be divided into two parts, *i.e.* $\varepsilon = \varepsilon_\mathrm{y} + \varepsilon_\mathrm{p}$, where ε_y is the yield strain at yield stress σ_y and ε_p is the effective strain beyond ε_y. So, in the case of $\sigma > \sigma_\mathrm{y}$, Eq. (1) can be represented as:

$$\sigma = \sigma_\mathrm{y}\left(1 + \frac{E}{\sigma_\mathrm{y}}\varepsilon_\mathrm{p}\right)^n \tag{2}$$

Here, it is worth noting that Poisson's ratio v is not an important factor in indentation experiments and for most engineering materials, $v \approx 0.3$[14]. Therefore, to fully determine elastic-plastic properties of a material, three independent parameters (*i.e.*, E, σ_y and n) should be known.

Although the indentation technique can date back to the work of Tabor[15] in 1951, the systemic study of obtaining three elastic-plastic parameters (E, σ_y and n) from a single indentation curve has been carried out in the recent decade. Based on the forward analysis for predicting the indentation response of a given set of elastic-plastic properties[16–18], Giannakopoulos *et al.*[9] introduced the reverse problem and proposed a comprehensive analytical framework. However, their work was developed by the small deformation finite element method, and in fact, deformation beneath indenter tip can reach 25–36% equivalent strain[19]. According to large deformation finite element results, Cheng and Cheng[20–22] derived a set of dimensionless functions that relate an indentation curve to elastic-plastic properties, but there was a lack of a full analytical framework to extract mechanical properties. Subsequently, Dao *et al.*[23] constructed universal forward and reverse analysis algorithms (referred to Dao model hereafter), which were verified by systematic experiments. However, there is still no consensus on whether elastic-plastic properties of a material can be uniquely determined by a single indentation curve. To analyze forward and reverse processes, Lu et al[24] considered about 9000 different combinations of elastic-plastic properties in seven representative methods. Chen et al[25] demonstrated the existence of "mystical materials", where materials with different elastic-plastic properties share almost the same *P-h* curves. Although many studies have been made on the uniqueness problem[22–26], there is not a suitable method to uniquely determine elastic-plastic properties of engineering materials by a simple indentation test. In this paper, uniqueness of the reverse algorithm in Dao model was studied by a mathematical method. The analysis was focused on dimensionless functions in the reverse procedure and their monotonic problems. Then, the sensitivity in prediction of n was discussed.

2. The reverse algorithm

Based on dimensionless analysis and large deformation finite element method, six dimensionless functions Π_1, Π_2, Π_3, Π_4, Π_5 and Π_6 were obtained, and then, a set of reverse analysis algorithm was established in Dao model[23]. The ranges of E, σ_y and n used in calculations and expressions of these dimensionless functions are given in Appendix A. Fig. 2 displays an adapted reverse analysis framework, which involves the following steps:

(1) Identify the ratio h_r / h_m from dimensionless function Π_5 according to the total work W_t and the plastic work W_p under an indentation curve.

(2) Using the contact stiffness S, the maximum load P_m and h_r / h_m, determine H and E^* from functions Π_4 and Π_6, where the reduced Young's modulus E^* is defined as, $E^* = [(1 - \nu^2)/E + (1-\nu_i^2)/E_i]^{-1}$, with subscript '$i$' being the indenter.

(3) With E^* being determined and C directly observed from the loading curve, calculate $\sigma_{0.033}$ from function Π_1, where $\sigma_{0.033}$ is the representative stress defined at strain $\varepsilon_r = \varepsilon_p = 0.033$. By using $\sigma_{0.033}$, the dimensionless function Π_1 was normalized to be independent of the strain hardening exponent n.

(4) Obtain h_m from the loading curve. Using the values of E^*, $\sigma_{0.033}$ and S obtained above, calculate n from function Π_2.

(5) Using E^*, $\sigma_{0.033}$ and n, calculate σ_y from Eq. (2).

3. Uniqueness of reverse analysis

According to the mathematical expressions of Π_1, Π_4 and Π_5, it is obvious that they are monotonic functions of $E^*/\sigma_{0.033}$ ($20 \le E^*/\sigma_{0.033} \le 770$ in [23]) and h_r / h_m, respectively. Rearranging dimensionless functions of Π_4 and Π_6 (in Fig. 2), we have:

$$H = \frac{S^2}{P_m}\left(\frac{\Pi_4}{\Pi_6}\right)^2 \tag{3}$$

$$E^* = \frac{\Pi_4}{P_m}\left(\frac{S}{\Pi_6}\right)^2 \tag{4}$$

Because Π_6 is a constant[23], H and E^* can be taken as a monotonic function of h_r / h_m. Following the steps (1)–(3), H, E^* and $\sigma_{0.033}$ can be uniquely determined. If n can be uniquely determined, σ_y is also unique. Thus, the key point of this uniqueness problem is how to determine n.

The dimensionless function Π_2 (Eq. (A2)) can be rewritten as:

$$an^3 + bn^2 + cn + d - \Pi_2 = 0 \tag{5}$$

where coefficients a, b, c and d are functions of $\ln(E^*/\sigma_{0.033})$. Denoting $n = N - b/3a$, Eq. (5) becomes

$$N^3 + \left(-\frac{b^2}{3a^2} + \frac{c}{a}\right)N + \frac{2b^3}{27a^3} - \frac{bc}{3a^2} + \frac{d - \Pi_2}{a} = 0 \tag{6}$$

where $a \neq 0$ (*i.e.*, $E^*/\sigma_{0.033} \neq 50$). Similarly, introducing two parameters p and q, Eq. (6) can be rearranged as

$$N^3 + pN + q = 0 \tag{7}$$

where $p = -\frac{b^2}{3a^2} + \frac{c}{a}$, and $q = \frac{2b^3}{27a^3} - \frac{bc}{3a^2} + \frac{d - \Pi_2}{a}$.

According to the Cardan formula[27], there are three roots (N_1, N_2, N_3) of Eq. (7). Thus, the three roots of Eq. (5) can be obtained as follows:

$$\begin{aligned} n_1 &= N_1 - \frac{b}{3a} = \sqrt[3]{T + \sqrt{D}} + \sqrt[3]{T - \sqrt{D}} - \frac{b}{3a} \\ n_2 &= N_2 - \frac{b}{3a} = \omega_1 \sqrt[3]{T + \sqrt{D}} + \omega_2 \sqrt[3]{T - \sqrt{D}} - \frac{b}{3a} \\ n_3 &= N_3 - \frac{b}{3a} = \omega_2 \sqrt[3]{T + \sqrt{D}} + \omega_1 \sqrt[3]{T - \sqrt{D}} - \frac{b}{3a} \end{aligned} \tag{8}$$

where $\omega_1 = \left(-1 + \sqrt{3}i\right)/2$, $\omega_2 = \left(-1 - \sqrt{3}i\right)/2$, $T = -q/2$, and $D = (q/2)^2 + (p/3)^3$ with $i = \sqrt{-1}$. Based on the characteristic features of these roots[27], the following conclusions can be proved: (1) when $D > 0$, there are one real root and two conjugate imaginary roots; (2) when $D = 0$, there are three real roots, in which at least two are unequal; and (3) when $D < 0$, there are three unequal real roots.

According to Eq. (6), to discuss the unique problem of n by using dimensionless function Π_2, the range of $E^*/\sigma_{0.033}$ can be divided into three intervals such as, 20–50, 50, and 50–770.

Case 1: 20 ≤ $E^*/\sigma_{0.033}$ < 50

A three-dimensional graphics of discriminant $D\left(E^*/\sigma_{0.033}, \Pi_2\right) = (q/2)^2 + (p/3)^3$ is shown in Fig. 3, from which two cross-sections (curves A and B in Fig. 4) were made with $D(E^*/\sigma_{0.033}, \Pi_2) = 0$. These two lines separate the area into three parts: two of them with $D > 0$ (*i.e.*, one real root), and the other with $D < 0$ (*i.e.*, three unequal real roots). Curves of dimensionless function $\Pi_2(E^*/\sigma_{0.033}, n)$ with $20 \leq E^*/\sigma_{0.033} < 50$ and n = 0, 0.1, 0.3, and 0.5 are also plotted in Fig. 4. Obviously, all the curves fall into an area of $D \leq 0$, implying that there are three real roots (n_1, n_2 and n_3) according to

the Cardan formula[27]. To distinguish the analytical expression in Eq. (8) that can be used to calculate the value of n, calculations were carried out by taking the values of $E^*/\sigma_{0.033}$ and Π_2 from Fig. 4. Let us take the curve $n = 0$ for example. As shown in Fig. 5(a), the calculated values of n_1 exceed 0.5, and thus the expression of n_1 would give a wrong solution. In the case of $20 \le E^*/\sigma_{0.033} \le 26$, the expression of n_2 yields a reasonable prediction of n, but an unreasonable, negative value of n_2 if $26 < E^*/\sigma_{0.033} < 50$. It is worth noting that, if $20 \le E^*/\sigma_{0.033} \le 26$, Eq. (8) has two reasonable n, *i.e.* n_2 and n_3. That is, n cannot be uniquely determined. Figs. 5(c)–(d) show the results with $n = 0.1$, 0.3, and 0.5, respectively. The non-uniqueness situation in calculating n also exists in the case of $20 \le E^*/\sigma_{0.033} \le 26$ and $n = 0.5$. Thus, except for the cases of $20 \le E^*/\sigma_{0.033} \le 26$, $0 \le n < 0.1$ and $0.3 < n \le 0.5$, one real value of n can be uniquely determined with the expression of n_3 in Eq. (8).

Case 2: $E^*/\sigma_{0.033} = 50$

In the case of $E^*/\sigma_{0.033} = 50$, Eq. (5) can be rewritten as:

$$0.02357n^2 - 1.25279n + 5.34692 - \Pi_2 = 0 \tag{9}$$

The two solutions of Eq. (9) are

$$\begin{aligned} n_1 &= 21.2145\left(1.25279 - 0.30704\sqrt{11.301 + \Pi_2}\right) \\ n_2 &= 21.2145\left(1.25279 + 0.30704\sqrt{11.301 + \Pi_2}\right) \end{aligned} \tag{10}$$

Since the range of Π_2 is from 4.72642 to 5.34692, it is obvious that the reasonable solution is n_1.

Case 3: $50 < E^*/\sigma_{0.033} \le 770$

A three-dimensional graphics of $D\left(E^*/\sigma_{0.033}, \Pi_2\right) = \left(q/2\right)^2 + \left(p/3\right)^3$ in the case of $50 < E^*/\sigma_{0.033} \le 770$ is shown in Fig. 6. The surface of discriminant D is also sectioned by using a plane of $D(E^*/\sigma_{0.033}, \Pi_2) = 0$, however, there is no cross curve in the $E^*/\sigma_{0.033}$ - Π_2 plane. All the discriminant values $D > 0$, namely, the solution of n is unique by using the expression of n_1 in Eq. (8) in all the cases of $50 < E^*/\sigma_{0.033} \le 770$.

Based on above discussion, non-uniqueness of n determined by Π_2 occurs in the case of $20 \le E^*/\sigma_{0.033} \le 26$, $0.3 < n \le 0.5$ and $0 \le n < 0.1$. However, the non-unique range in Dao model is just in the domain of $20 \le E^*/\sigma_{0.033} \le 26$, $0.3 < n \le 0.5$[23]. Lan *et al.*[24] obtained the similar non-unique

domain based on about 9000 different combinations of elastic-plastic properties (there are only 76 different combinations in Dao model), which is $20 \le E^*/\sigma_{0.033} \le 26$ and $0.37 < n \le 0.5$. Obviously, the range of n is less than that of Dao model. Compared with Dao and Lan's results, a new non-unique domain of $20 \le E^*/\sigma_{0.033} \le 26$ and $0 \le n < 0.1$ is obtained.

Dao *et al.*[23] found out that the single solution of n could be obtained by using dimensionless function Π_3 instead of Π_2. Similar to the analysis of Π_2, the mathematical expression of Π_3 (Eq. (A3)) can be rearranged as:

$$a'n^2 + b'n + c' - \Pi_3 = 0 \tag{11}$$

where coefficients a', b', c' and d' are functions of $\ln(\sigma_{0.033}/E^*)$. The roots of Eq. (11) can be expressed as

$$\begin{aligned} n_1^* &= \frac{-b' + \sqrt{\Delta}}{2a'} \\ n_2^* &= \frac{-b' - \sqrt{\Delta}}{2a'} \end{aligned} \tag{12}$$

where $\Delta = \Delta\left(\sigma_{0.033}/E^*, \Pi_3\right) = b'^2 - 4a'(c' - \Pi_3)$. A three-dimensional graphics of discriminant $\Delta\left(\sigma_{0.033}/E^*, \Pi_3\right)$ is plotted in Fig. 7, in which two curves A and B (see Fig. 8) are sectioned with $\Delta = 0$. They separate the area into three regions: two of them with $\Delta < 0$ and the other with $\Delta > 0$. It is worth noting that all the curves of dimensionless function Π_3 (see Fig. 10 (b) in [23]) fall into the region of $\Delta \ge 0$. That is, there are two real solutions of Eq. (12). As shown in Fig. 9, one real value of n can be uniquely determined with the expression of n_2^* for all the range of $\sigma_{0.033}$ / E^*. Furthermore, if $\sigma_{0.033}$ / E^* is very small (especially less than 0.005), all the curves of n = 0, 0.1, 0.3 and 0.5 are too close to be distinguished. Thus, n is mainly determined by dimensionless function Π_2, and only in the case of $20 \le E^*/\sigma_{0.033} \le 26$, $0.3 < n \le 0.5$ and $0 \le n < 0.1$, dimensionless function Π_3 can be used.

4. Sensitivity analysis in the prediction of *n*

According to uniqueness analysis, the non-unique domains in determining n are quite inconsistent with that in Dao model. Therefore, it is necessary to conduct a particular sensitivity analysis in the prediction of n. The experimental errors cannot be avoided and small variations in experiments may influence largely the values of Π_2 and Π_3. Here, a $\pm 2\%$ variation of Π_2 or Π_3 is assumed in analyzing the corresponding variation of n.

As shown in Fig. 10, it is seen that variations of n in Eq. (8) are within 7% in the case of $50 < E^*/\sigma_{0.033} \leq 770$. If $26 < E^*/\sigma_{0.033} \leq 50$, n can be uniquely determined by n_3 in Eq. (8) based on Π_2. However, based on sensitivity analysis, there is an unacceptable variation (almost 100%) in the prediction of n. Hence, Π_3 is applied to predict n in the case of $26 < E^*/\sigma_{0.033} \leq 50$.

In the case of $20 \leq E^*/\sigma_{0.033} \leq 50$, a unique solution of n can be obtained using dimensionless function Π_3. Figure 11 illustrates the variations of n caused by a change of $\pm 2\%$ in Π_3 for $n_0 = 0.15$, 0.3, and 0.5, respectively. It is obvious that n seems insensitive to uncertainty in Π_3 and varies within $n_0 \pm 0.15$ if $n_0 > 0.15$. However, for low hardening materials ($n_0 \leq 0.15$), prediction values of n are sensitive to an error of $\pm 2\%$ in Π_3 and unreliable. This is not surprising because, when $20 \leq E^*/\sigma_{0.033} \leq 50$ and $n_0 \leq 0.15$, the curves of dimensional function $\Pi_3(\sigma_{0.033}/E^*)$ as shown in Fig. 8, are close to each other and also to the region of $\Delta < 0$ (no real root).

5. Conclusion

In this paper, six dimensionless functions in the reverse algorithm proposed in Dao model have been analyzed. The main results are summarized as follows:

(1) Young's modulus E and hardness H can be uniquely determined by an indentation curve, and if the strain hardening exponent n is known, the yield strength σ_y can also be uniquely determined.

(2) The non-uniqueness problem happens in calculation of the strain hardening exponent n. Besides the range of $E^*/\sigma_{0.033} \leq 26$ and $0.3 < n \leq 0.5$ mentioned in Dao model, non-uniqueness also exists in the case of $20 \leq E^*/\sigma_{0.033} \leq 26$ and $0 \leq n < 0.1$, which can be solved by using dimensionless function Π_3 instead of Π_2.

(3) Sensitivity analysis show that, in the case of $26 < E^*/\sigma_{0.033} \leq 50$, n is highly sensitive to Π_2, and in the case of $20 \leq E^*/\sigma_{0.033} \leq 50$ and $n \leq 0.15$, n is sensitive to Π_3.

Acknowledgements

This work was supported by the National Natural Science Foundation of China (Nos. 11002121, 11002122, and 10828205), the Natural Science Foundation of Hunan Province for Innovation Group (No. 09JJ7004), the Key Special Program for Science and Technology of Hunan Province (No. 2009FJ1002), and the Natural Science Foundation of Xiangtan University (No. 09XZX04). One of the authors (C. Lu) is also grateful to the support from the Australian Research Council (No. DP0985450).

REFERENCES

[1] S. M. Spearing: *Acta Mater.*, 2000, **48**: 179.

[2] S. P. Baker: *Mater. Sci. Eng. A.*, 2001, **319-321**: 16.

[3] H. D. Espinosa, B. C. Prorok and M. Fischer: *J. Mech. Phys. Solids*, 2003, **51**: 47.

[4] S. F. Hwang, J. H. Yu, B. J. Lai and H. K. Liu: *Mech. Mater.*, 2008, **40**: 658.

[5] D. Kiener, C. Motz, T. Schöberl, M. Jenko and G. Dehm: *Adv. Eng. Mater.*, 2006, **8**: 1119

[6] J. Vlassak and W. J. Nix: *J. Mater. Res.*, 1992, **7**: 401.

[7] W. C. Oliver and G. M. Pharr: *J. Mater. Res.*, 1992, **7**: 1564.

[8] N. Huber and J. Heerens: *Acta Mater.*, 2008, **56**: 6205.

[9] A. E. Giannakopoulos and S. Suresh: *Scripta Mater.*, 1999, **40**: 1191.

[10] Y. G. Liao, Y. C. Zhou, Y. L. Huang and L. M. Jiang: *Mech. Mater.*, 2009, **41**: 308.

[11] T. Y. Tsui and G. M. Pharr: *J. Mater. Res.*, 1999, **14**: 292.

[12] R. Saha and W. D. Nix: *Acta Mater.*, 2002, **50**: 23.

[13] Y. T. Cheng and C. M. Cheng: *Mater. Sci. Eng.*, 2004, **R44**: 91.

[14] Y. T. Cheng and C. M. Cheng: *Int. J. Solids Struct*., 1999, **36**: 1231.

[15] D. Tabor: *The hardness of metals*, Clarendon Press, Oxford, 1951, 6.

[16] A. E. Giannakopoulos, P. -L. Larson, and R. Vestergaard: *Int. J. Solids Struct.*, 1994, **31**: 2679.

[17] A. E. Giannakopoulos and P. -L. Larson: *Mech. Mater.*, 1997, **25**: 1.

[18] P. L. Larson, A. E. Giannakopoulos, E. Soderlund, D. J. Rowcliffe and R. Vestergaard: *Int. J. Solids Struct.*, 1996, **33**: 221.

[19] M. M. Chaudhri: *Acta Mater.*, 1998, **46**: 3047.

[20] Y. T. Cheng and C. M. Cheng: *J. Appl. Phys.*, 1998, **84**: 1284.

[21] Y. T. Cheng and C. M. Cheng: *Appl. Phys. Lett.*, 1998, **73**: 614.

[22] Y. T. Cheng and C. M. Cheng: *J. Mater. Res.*, 1999, **14**: 3493.

[23] M. Dao, N. Chollacoop, K. J. Van vliet, T. A. Venkatesh and S. Suresh: *Acta Mater.*, 2001, **49**: 3899.

[24] H. Lan and T. A. Venkatesh: *Philos. Mag.*, 2007, **87**: 4671.

[25] X. Chen, N. Ogasawara, M. H. Zhao and N. Chiba: *J. Mech. Phys. Solids*, 2007, **55**: 1618.

[26] N. Ogasawara, N. Chiba and X. Chen: *Scripta Mater.*, 2006, **54**: 65.

[27] X. G. Xiao, J. Y. Zhu, S. Z. Yang and S. P. Yang: *A mathematical handbook for college students*, Tianjin Science and Technology Press, Tianjin, 1995, 11.

APPENDIX A

The six dimensionless functions (Π_1~Π_6) in Dao model are based on a parametric study of 76 cases, which cover mechanical properties of engineering metals with E from 10 to 210 GPa, σ_y from 30 to 3000 MPa, and n from 0 to 0.5. Their detailed expressions are listed below:

$$\Pi_1 = \frac{C}{\sigma_{0.033}} = -1.131\left[\ln\left(\frac{E^*}{\sigma_{0.033}}\right)\right]^3 + 13.635\left[\ln\left(\frac{E^*}{\sigma_{0.033}}\right)\right]^2 - 30.594\left[\ln\left(\frac{E^*}{\sigma_{0.033}}\right)\right] + 29.267 \quad \text{(A1)}$$

$$\begin{aligned}\Pi_2\left(\frac{E^*}{\sigma_{0.033}}, n\right) &= \frac{S}{E^* h_m} \\ &= \left(-1.40557n^3 + 0.77526n^2 + 0.15830n - 0.06831\right)\left[\ln\left(\frac{E^*}{\sigma_{0.033}}\right)\right]^3 \\ &+ \left(17.93006n^3 - 9.22091n^2 - 2.37733n + 0.86295\right)\left[\ln\left(\frac{E^*}{\sigma_{0.033}}\right)\right]^2 \\ &+ \left(-79.99715n^3 + 40.5562n^2 + 9.00157n - 2.54543\right)\left[\ln\left(\frac{E^*}{\sigma_{0.033}}\right)\right] \\ &+ 122.65069n^3 - 63.88418n^2 - 9.58936n + 6.20045\end{aligned} \quad \text{(A2)}$$

$$\begin{aligned}\Pi_3\left(\frac{\sigma_{0.033}}{E^*}, n\right) &= \frac{h_r}{h_m} \\ &= \left(0.0101n^2 + 0.0017639n - 0.0040837\right)\left[\ln\left(\frac{\sigma_{0.033}}{E^*}\right)\right]^3 \\ &+ \left(0.14386n^2 + 0.018153n - 0.088198\right)\left[\ln\left(\frac{\sigma_{0.033}}{E^*}\right)\right]^2 \\ &+ \left(0.59505n^2 + 0.034074n - 0.65417\right)\left[\ln\left(\frac{\sigma_{0.033}}{E^*}\right)\right] \\ &+ 0.5818n^2 - 0.08846n - 0.6729\end{aligned} \quad \text{(A3)}$$

$$\Pi_4 = \frac{H}{E^*} \approx 0.268536\left(0.9952495 - \frac{h_r}{h_m}\right)^{1.1142735} \quad \text{(A4)}$$

$$\Pi_5 = \frac{W_p}{W_t} = 1.61217\left\{1.13111 - 1.74756^{\left[-1.49291\left(\frac{h_r}{h_m}\right)^{2.535334}\right]} - 0.075187\left(\frac{h_r}{h_m}\right)^{1.135826}\right\} \quad \text{(A5)}$$

$$\Pi_6 = \frac{S}{E^*}\sqrt{\frac{H}{P_m}} \quad \text{(A6)}$$

Figure captions

Fig. 1 Schematic of a typical load-displacement curve of an elastic-plastic material by sharp indentation.

Fig. 2 Illustration of an adapted reverse analysis algorithm.

Fig. 3 Three-dimensional graphics of discriminant $D(E^*/\sigma_{0.033}, \Pi_2)$ if $20 \le E^*/\sigma_{0.033} < 50$.

Fig. 4 Curves sectioned from Fig. 3 by a plane of $D(E^*/\sigma_{0.033}, \Pi_2) = 0$ and dimensionless function $\Pi_2(E^*/\sigma_{0.033}, n)$ in the case of $20 \le E^*/\sigma_{0.033} < 50$ and $n = 0$, 0.1, 0.3, 0.5.

Fig. 5 Calculated results of n_1, n_2 and n_3 for curves with (a) $n = 0$, (b) $n = 0.1$, (c) $n = 0.3$, and (d) $n = 0.5$.

Fig. 6 Three-dimensional graphics of discriminant $D(E^*/\sigma_{0.033}, \Pi_2)$ if $50 < E^*/\sigma_{0.033} \le 770$.

Fig. 7 Three-dimensional graphics of discriminant $\Delta\left(\sigma_{0.033}/E^*, \Pi_3\right)$.

Fig. 8 Curves sectioned from Fig. 7 and dimensionless function $\Pi_3(\sigma_{0.033}/E^*, n)$.

Fig. 9 Calculated results of n_1^* and n_2^* for curves with $n = 0$, 0.1, 0.3, and 0.5, respectively.

Fig. 10 Variations of n caused by a change of $\pm 2\%$ in Π_2 for $n_0 = 0$, 0.1, 0.3, and 0.5 in the case of $50 < E^*/\sigma_{0.033} \le 770$, where n_0 is the real value without input error.

Fig. 11 Variations of n caused by a change of $\pm 2\%$ in Π_3 for $n_0 = 0.15$, 0.3, and 0.5 in the case of $0.02 \le \sigma_{0.033}/E^* \le 0.05$ (*i.e.*, $20 \le E^*/\sigma_{0.033} \le 50$).

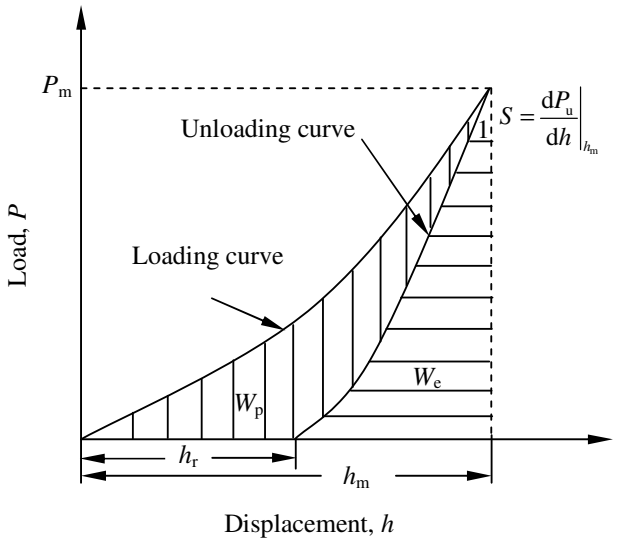
P_m
Unloading curve
$S = \left.\frac{dP_u}{dh}\right|_{h_m}$
1
Load, P
Loading curve
W_e
W_p
h_r
h_m
Displacement, h

Fig. 1

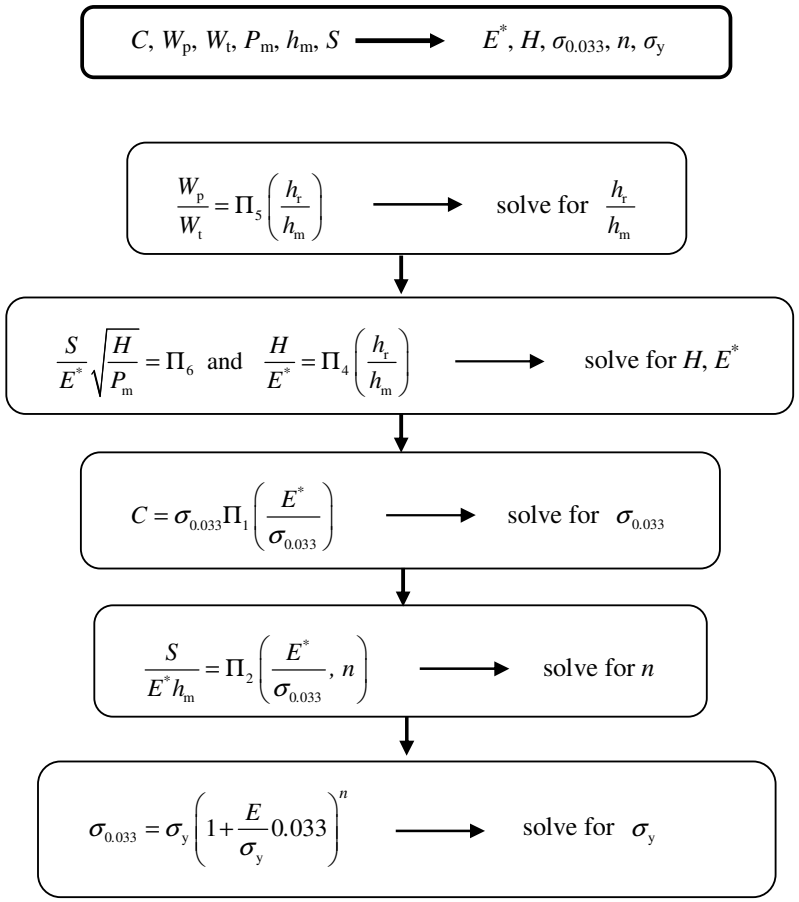
C, W_p, W_t, P_m, h_m, S → E^*, H, $\sigma_{0.033}$, n, σ_y
$\frac{W_p}{W_t} = \Pi_5\left(\frac{h_r}{h_m}\right)$ → solve for $\frac{h_r}{h_m}$
$\frac{S}{E^*}\sqrt{\frac{H}{P_m}} = \Pi_6$ and $\frac{H}{E^*} = \Pi_4\left(\frac{h_r}{h_m}\right)$ → solve for H, E^*
$C = \sigma_{0.033}\Pi_1\left(\frac{E^*}{\sigma_{0.033}}\right)$ → solve for $\sigma_{0.033}$
$\frac{S}{E^* h_m} = \Pi_2\left(\frac{E^*}{\sigma_{0.033}}, n\right)$ → solve for n
$\sigma_{0.033} = \sigma_y\left(1 + \frac{E}{\sigma_y}0.033\right)^n$ → solve for σ_y

Fig. 2

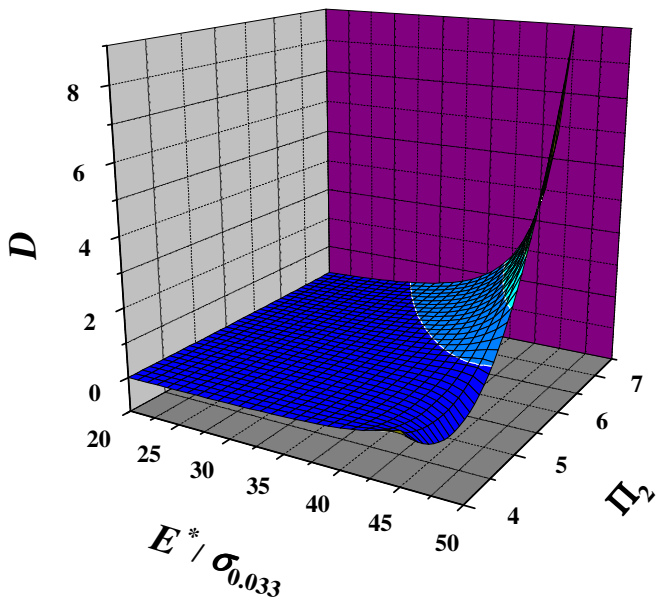

Fig. 3

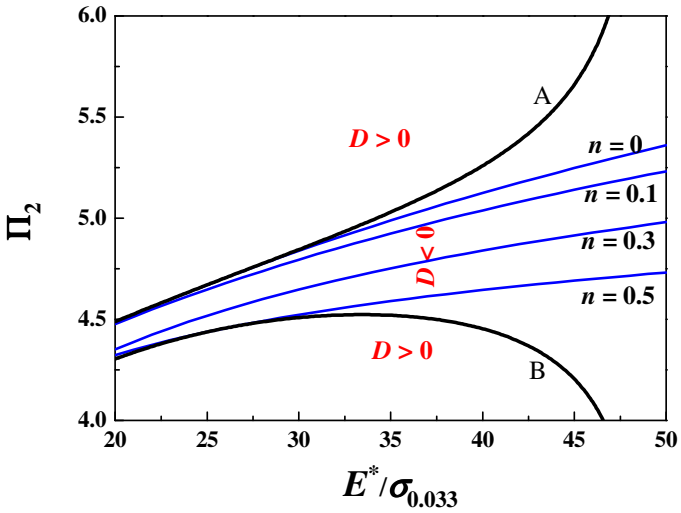
6.0
5.5
5.0
4.5
4.0
20
25
30
35
40
45
50
Π_2
$E^*/\sigma_{0.033}$
A
B
D > 0
D > 0
D < 0
n = 0
n = 0.1
n = 0.3
n = 0.5

Fig. 4

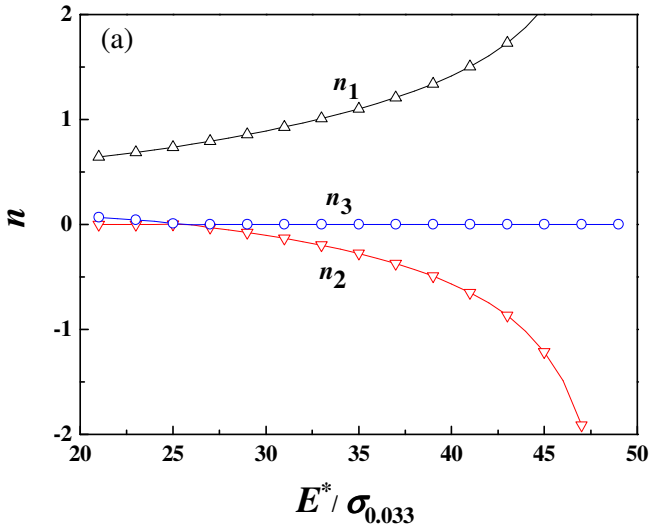

Fig. 5(a)

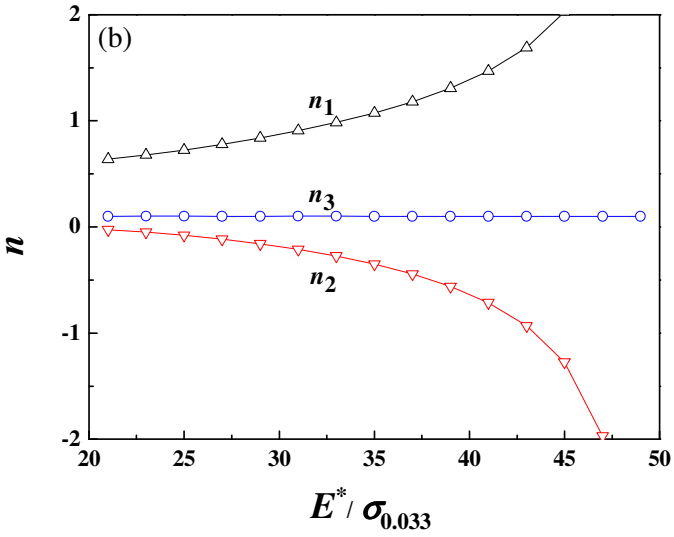

Fig. 5(b)

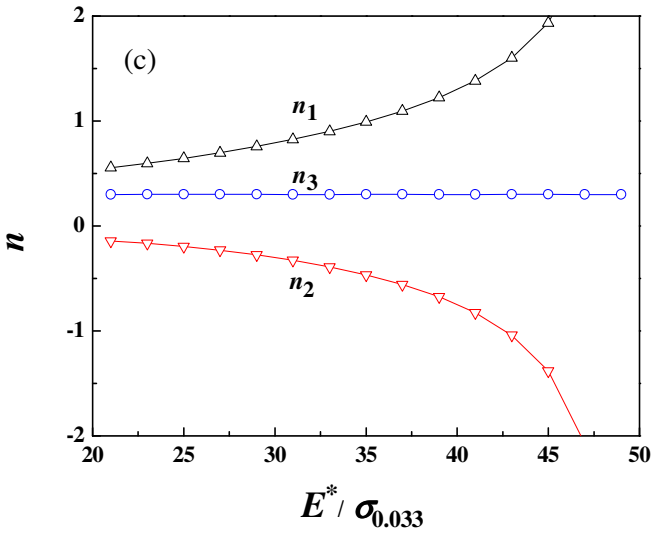

Fig. 5(c)

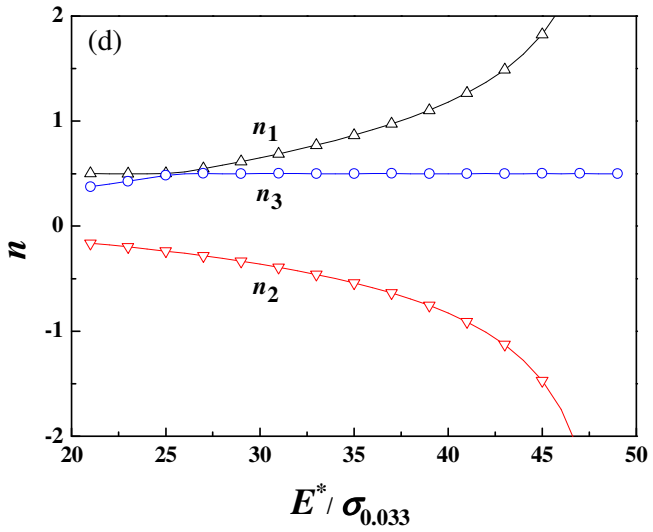

Fig. 5(d)

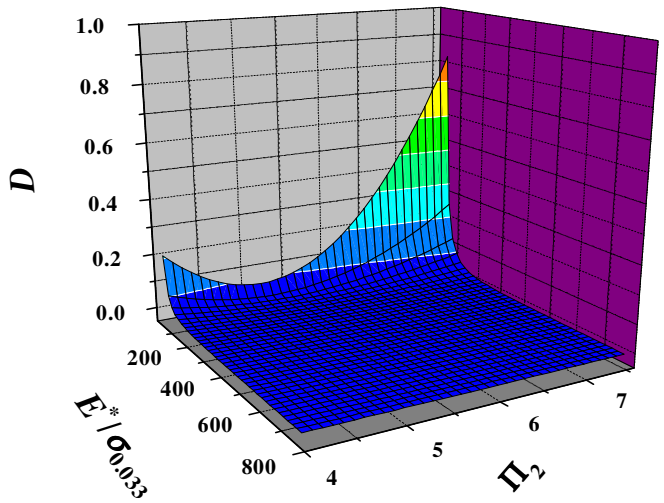

Fig. 6

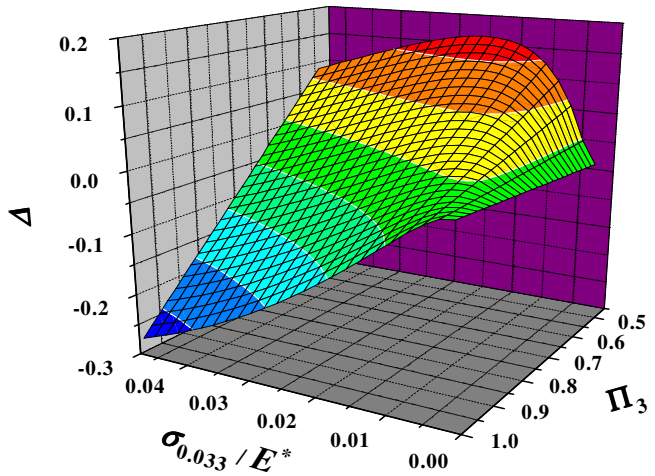

Fig. 7

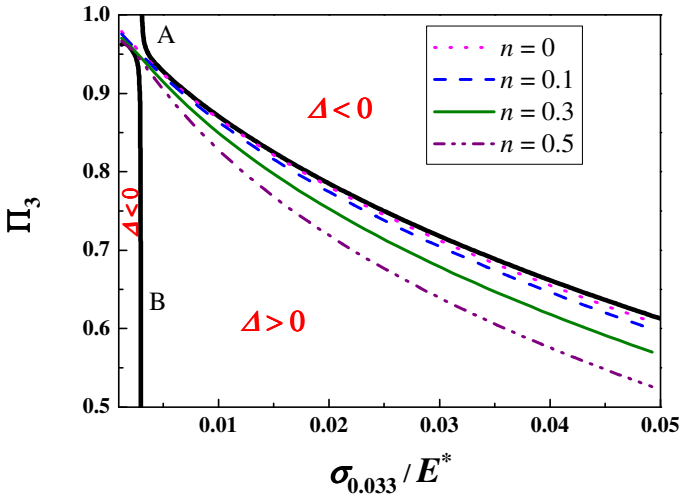
1.0
0.9
0.8
0.7
0.6
0.5
Π_3
A
B
$n = 0$
$n = 0.1$
$n = 0.3$
$n = 0.5$
$\Delta < 0$
$\Delta > 0$
$\Delta < 0$
0.01
0.02
0.03
0.04
0.05
$\sigma_{0.033} / E^*$

Fig. 8

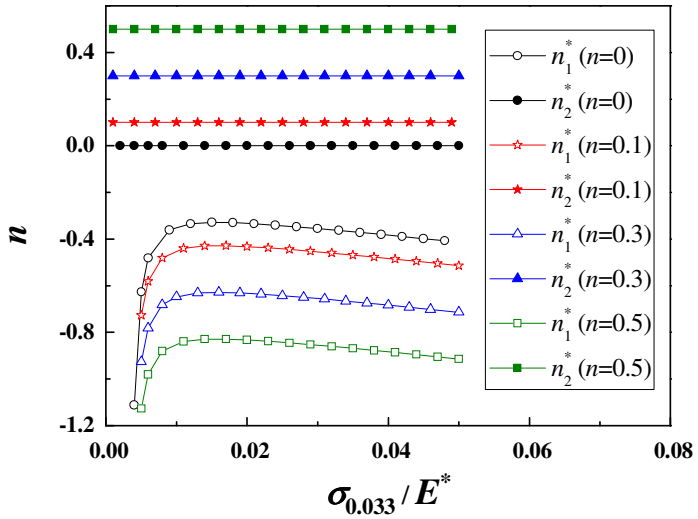
0.4
0.0
-0.4
-0.8
-1.2
n
0.00
0.02
0.04
0.06
0.08
$\sigma_{0.033} / E^*$
n_1^* (n=0)
n_2^* (n=0)
n_1^* (n=0.1)
n_2^* (n=0.1)
n_1^* (n=0.3)
n_2^* (n=0.3)
n_1^* (n=0.5)
n_2^* (n=0.5)

Fig. 9

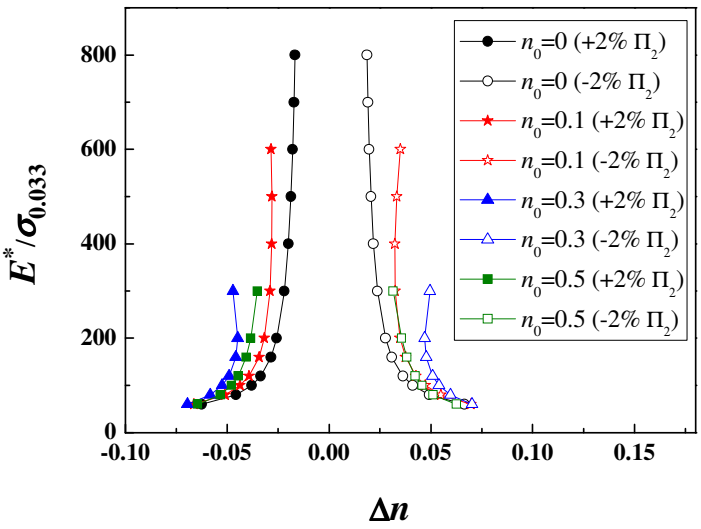
$E^*/\sigma_{0.033}$
800
600
400
200
0
-0.10
-0.05
0.00
0.05
0.10
0.15
Δn
n_0=0 (+2% Π_2)
n_0=0 (-2% Π_2)
n_0=0.1 (+2% Π_2)
n_0=0.1 (-2% Π_2)
n_0=0.3 (+2% Π_2)
n_0=0.3 (-2% Π_2)
n_0=0.5 (+2% Π_2)
n_0=0.5 (-2% Π_2)

Fig. 10

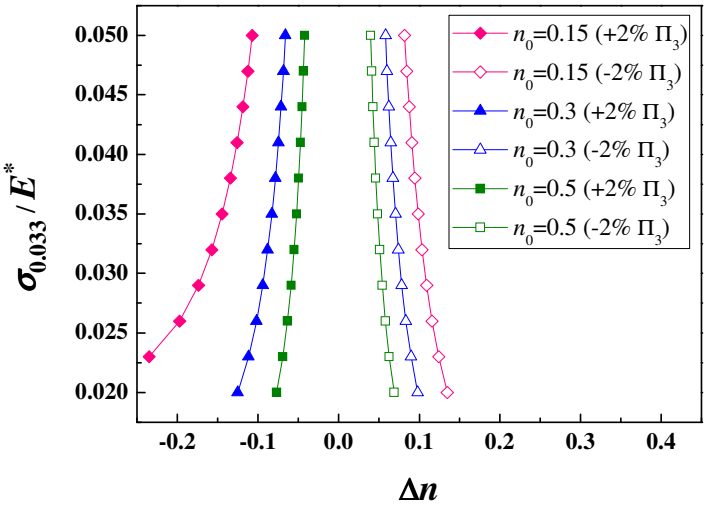
0.050
0.045
0.040
0.035
0.030
0.025
0.020
-0.2
-0.1
0.0
0.1
0.2
0.3
0.4
$\sigma_{0.033}/E^*$
Δn
n_0=0.15 (+2% Π_3)
n_0=0.15 (-2% Π_3)
n_0=0.3 (+2% Π_3)
n_0=0.3 (-2% Π_3)
n_0=0.5 (+2% Π_3)
n_0=0.5 (-2% Π_3)

Fig. 11